Design of RC joints equipped with hybrid trussed beams and friction dampers

Design of RC joints equipped with hybrid trussed beams and friction dampers

Piero Colajanni[a,1], Lidia La Mendola[a,2], Alessia Monaco[b,3*], Salvatore Pagnotta[a,4]

[a] *Department of Engineering, University of Palermo, Viale delle Scienze, Edificio 8 - 90128 Palermo, Italy*

[b] *Department of Architecture and Design, Politecnico di Torino, Viale Mattioli 39 - 10125 Torino, Italy*

[1]*piero.colajanni@unipa.it*, [2]*lidia.lamendola@unipa.it*, [3]*alessia.monaco@polito.it*, [4]*salvatore.pagnotta@unipa.it*

[*]Corresponding author: Alessia Monaco, Department of Architecture and Design, Politecnico di Torino, Viale Mattioli 39 - 10125 Torino, Italy, e-mail: alessia.monaco@polito.it

HIGHLIGHTS:

- Innovative design strategies of multi-storey framed structures in seismic area using friction devices
- Feasibility study for the application of friction dampers to partially prefabricated RC structures
- Performance of RC joints with hybrid trussed beams and concrete colums equipped with friction devices
- Friction dampers prevent the damage of main structural elements and limit the panel zone cracking
- Numerical modeling of the novel hybrid beam-to-column joint under cyclic actions

ABSTRACT

The challenge of this research consists in the first attempt to apply a dissipative friction connection to beam-to-column joints with semi-prefabricated Hybrid Steel-Trussed Concrete Beams (HSTCB) and RC pillars cast in-situ. Nowadays, HSTCBs are widely adopted in civil and industrial buildings and, therefore, it is required to evaluate their compliance with the capacity design criteria and their seismic energy dissipation capability. However, the design of the reinforcement of such beams usually lead to the adoption of large amount of steel within the panel zone which becomes potentially vulnerable to the effects of seismic cyclic actions and dramatically reduce the dissipation capacity of the entire structure. Therefore, the introduction of friction dampers in the HSTCB-to-column joints is investigated in order

to evaluate the ability of the device in preventing the main structural elements from damage and limiting the cracking of the panel zone, thanks to the increase of the bending moment lever arm, which reduces the shear forces in the joint. Moreover, the proposed solution thoroughly investigates the connection between the friction device and the beam in order to ensure adequate strength and stiffness to the connection. The feasibility study is firstly conducted through the development of design criteria for the pre-dimensioning of the device and, successively, the proposed solution is validated through the generation of finite element models.

KEYWORDS: friction dampers; hybrid steel-trussed-concrete beams; cyclic behaviour; RC joints; finite element models; structural design; earthquake design; seismic energy dissipation.

1 INTRODUCTION

The most recent design strategies of multi-storey framed structures are increasingly welcoming the adoption of innovative techniques for the seismic energy mitigation, in order to guarantee a highly dissipative global behaviour able to prevent the structure from collapse with consequent loss of human lives. In particular, there is a large interest in the study of those devices able to absorb the whole seismic energy avoiding the damage of the primary load-bearing structural elements. Thus, irreversibly damage after a violent seismic event, resulting in extremely high economic costs for their structural repair is avoided. Several friction damper devices have been proposed over the last two decades. Solutions for steel structures have been developed mainly in New Zealand, and in Italy. The Sliding Hinge Joint with Asymmetric Friction Connection was proposed in New Zealand; this friction device is constituted by the bottom flange of the beam, a steel plate welded to the column flange and a cap plate able to double the friction force once a certain rotation of the connection is achieved [1-3]. In Italy, two replaceable friction connections for beam-to-column joints have been proposed, characterized by friction devices arranged in the horizontal or vertical direction and belonging to a haunch bolted to the bottom flange of the beam, able to increase the internal lever arm of the moment transferred to the column [4,5]. Concerning concrete structures, few applications have been proposed, especially for prefabricated structures (e.g. [6-8]).

In the last thirty years, Hybrid Steel-Trussed-Concrete Beams (HSTCBs) have been widely used in civil and industrial buildings and, therefore, their mechanical performance must be evaluated for ensuring the compliance with the capacity design criteria and achieving the adequate amount of seismic energy dissipation, particularly in the beam-to-column joints. HSTCBs' flexural and shear behaviour has been thoroughly studied through experimental tests, numerical models and analytical procedures. In particular, specimens of two-span continuous beams were tested under monotonic and cyclic actions in a three-point bending test with the aim of investigating the behaviour of the end-zone of the beam integrated into a moment resisting frame [9]. Moreover, experimental tests have been conducted on in-scale specimens for studying the cyclic behaviour of beam-to-column joints of framed RC structures with HSTCBs connected to RC piers, subjected to seismic actions, with the aim of verifying the dissipation capacity of the panel zone and the strength capacity and ductility of the entire system [10]. In both cases, the results proved that in the joint region the bottom steel plate and the top chord of the beam are not effective in tension, while they are partially effective in compression; moreover, in the absence of specific confining reinforcement at the beam-end, when large rotations are experienced, the damage of unconfined concrete reduces the strength of the section and the ductility for cyclic action, causing a sudden loss of bonding between reinforcing rebars and damaged concrete. The shear response of HSTCBs has been experimentally investigated performing three-point bending tests on specimens whose span-to-depth ratio was designed for exhibiting shear failure and comparing the results with several analytical shear models available in the codes and in the technical literature [11]. Numerical simulations of such tests were also developed to analyse in detail the failure modes and the stress transfer mechanism, using 3D FEM models with a damaged concrete and steel-concrete interface [12]. Numerical simulations were also developed to investigate the shear connection capacity through modelling of the push-out test response of specimens of HSTCB, several parametric analyses also being performed to study the influence of the most relevant geometrical and mechanical parameters (such as diameter of rebars, thickness of the bottom steel plate; concrete strength; steel grade) [13]. Analytical models were formulated to interpret the resisting mechanism of this beam typology with particular regard to the shear connection capacity, proposing a model based on the extension of existing formulations for prediction of

the resistance of steel dowels to the case of inclined steel bars loaded against concrete, accounting for several effects such as lateral and top confinement, mechanical nonlinearities, length of plastic hinge in the steel bar and moment-shear-axial force interaction. The experimental and numerical outcomes of the push-out test response were also exploited for model validation [14,15].

HSTCBs are often designed to exploit the steel reinforcement made up of a steel truss in order to cover large spans with reduced depth. In such cases, a large amount of steel reinforcement is required within the panel zone which is often made using large diameter rebar. These features make both the end of the beam and the joint potentially vulnerable to the effects of cyclic actions induced by the earthquake and dramatically reduce the dissipation capacity of the entire structure [9,16].

The challenge of this research consists in the first attempt to apply a dissipative friction connection to beam-to-column joints with semi-prefabricated Hybrid Steel-Trussed Concrete Beams (HSTCB) and RC pillars cast in-situ. The proposed solution thoroughly investigates the connection between the friction device and the beam in order to ensure adequate strength and stiffness to the connection. In particular, the solution adopted prevents several phenomena, such as damage to the concrete and steel reinforcement of the beam in the nodal area, buckling of the bottom steel plate of the beam, and loss of stiffness of the connection between device and beam. Furthermore, the use of curved slotted holes in the friction device and the design of a weakened T-stub section allows precise identification of the rotation centre of the device, obtaining non-degrading hysteresis cycles with constant strength throughout the operating range of the device. The design procedure, based on a suitable overstrength coefficient, makes it possible to cope with the uncertainties related to the values of both friction coefficient and preload acting on the bolts used in the friction device. Adoption of a vertical friction device, by increasing the internal lever arm, is able to reduce the forces transmitted to the columns, if compared to those transmitted by HSTCBs with standard connections, limiting damage to the panel zone and enhancing its cyclic performance [10]. The feasibility study is firstly conducted through the development of design criteria for the pre-dimensioning of the device and, successively, the proposed solution is validated through the generation of finite element models. Concerning the seismic behaviour of RC frames realized with HSTCBs and endowed with the proposed connection, this is currently being studied in other researches by the Authors.

2 DESIGN CRITERIA

The dissipative connection system between R.C. column and HSTCB represented in Fig. 1 is constituted by the following components: - the upper T-stub connection anchored to the column and bolted to a "C" steel profile which is welded to the upper longitudinal rebars of the steel truss of the HSTCB; - the friction connection on the bottom, constituted by a vertical central steel plate with curved slotted holes and steel angles anchored to the column; the latter realize the friction connection with the central slotted plate and eventual plies of friction material. These elements are connected by high strength friction bolts properly preloaded according to the slip force required.

T-stub and steel angles are designed to be carefully assembled in a factory, in order to ensure the correct clearance between bolt shanks and curved slotted holes. The connection between column and steel elements is realized by using long bolts; if the bond between long bolts and concrete is adequately guaranteed, the deformability of the connection should not exceed the deformability of a traditional connection generally made with smaller diameter rebars, characterized by a reduced internal lever arm, and thus subjected to higher axial forces.

The construction tolerances are taken into account at the connection between column and steel elements (T stub and steel angles). Vertical tolerance can be solved by realizing vertical slotted holes on the steel plates used for connecting the device to the column. Conversely, for horizontal tolerance, the device should be positioned before concrete casting of the column in order to accommodate the tolerance. The steel truss of the beam is made shorter in the factory (as is done today as well) than the effective span and the remaining length (about 5-10 cm) is completed by cast-in-situ concrete (if the panel zone and the beam are cast together) or by cement grout (if the panel zone and the beam are cast at different times). A detailed evaluation of the tolerances adopted for placing the device in situ and the characteristics of the disk springs used to keep the bolt preload constant are topics worthy of further study, and which play a decisive role in effective use of the device, but fall outside the scope of this work. Moreover, as regards the undesired influence of the slab on the overall behaviour of the connection as well on the impacts on

the required tolerance of the slots, in the literature some suggestions have been made for effectively disconnecting the slab from the joint ([17] and [18]), and friction devices have been proposed that by coupling horizontal and vertical slots, are able to accommodate the imperfections of the device (e.g. [5]). However, identification of efficient technical solutions for minimizing the effects of slab interaction is still a challenge in the scientific literature, worthy of further study and dedicated studies.

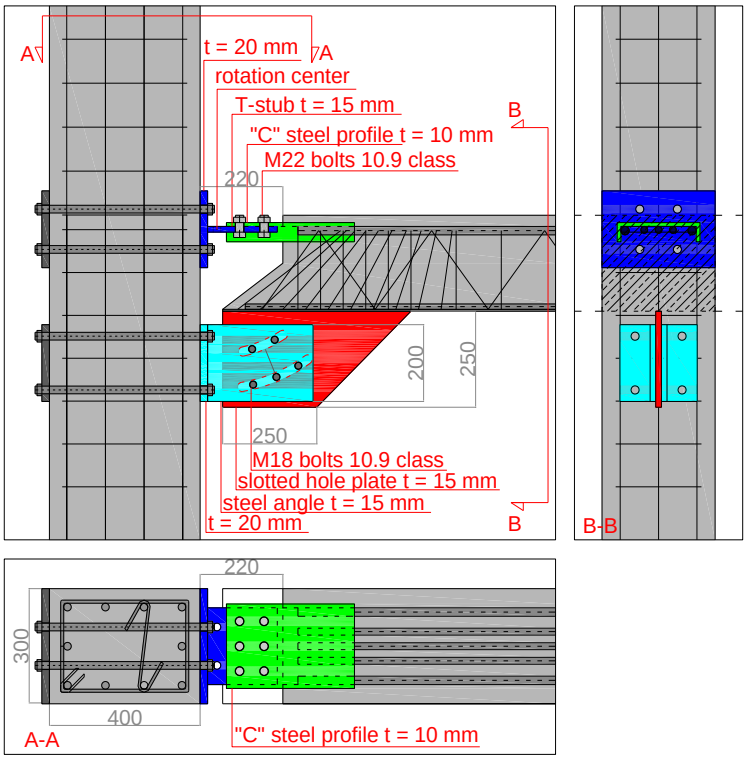

Fig. 1. Structural solution adopted for the connection.

2.1 Calculation of the design parameters

The design of the friction connection requires the definition of the design bending moment M_d which corresponds to the slippage of the device. Such a solicitation should be calculated from the structural analysis of the frame in which the friction connection needs to be used. The main scope is avoiding the slip of the device within the service limit state and allowing the dissipation under seismic events. With regard to the design of the geometry of the friction connection, an iterative procedure aiming at minimizing the height of the vertical central plate has been adopted, which can be summarized as follows: a tentative value of the internal lever arm *z* of the beam-to-column connection is selected according to both design moment strength and geometrical and mechanical properties of the beam (e.g. 1.5 times the

effective depth of the beam). Then the number and the diameter of the bolts required to obtain the design moment strength is calculated. Subsequently, the geometries of the vertical central plate, steel angles, and curved slotted holes are determined on the basis of the minimum distances between holes and edges of the plates, as suggested by Eurocode 3 [19,20]. In addition, the distance between vertical central plate and column as well as between steel angle and bottom plate must be adequate to accommodate the maximum rotation achievable by the connection, in order to prevent any undesired contact. If the above-mentioned prescriptions are satisfied, then the selected value of *z* might be greater than the minimum one and might be reduced until the optimal solution is found. By contrast, if only one of the prescriptions is not verified, then *z* is shorter than the optimal one and a new iteration has to be performed.

In this paper, a theoretical feasibility study is conducted and the specific structural details of the construction are not taken into account. Therefore, a design value of the bending moment is arbitrarily assumed M_d=110 kNm. Moreover, with the aim of providing overstrength to all components of the friction connection with respect to the load able to activate the slippage, an overstrength coefficient Ω_μ is adopted. In the absence of experimental campaigns for the assessment of the characteristic values of the static and dynamic friction coefficient, in this study the value Ω_μ = 1.5 is assumed. Therefore, the overstrengthened design bending moment is equal to $M_{Rd} = \Omega_\mu M_d$ = 1.5x110 = 165 kNm and, assuming a length L of 5m for the beam, the shear resistance results $V_{Rd} = 2M_{Rd}/L$ = 66 kN in the absence of distributed loads.

The friction damper is designed to withstand a tensile slip force F_d equal to the design bending moment M_d divided by the lever arm *z*, obtained via the above-mentioned iterative procedure, which is equal to 380 mm in our conception of the geometry of the device, which will be described more in detail later:

$$F_d = \frac{M_d}{z} = \frac{110}{0.38} = 289.5\ kN \tag{1}$$

It is assumed to use five M18 bolts 10.9 class, whose area is A_{res}=192 mm^2 and yielding and ultimate strength are f_{yb}=900 MPa and f_{ub}=1000 MPa. Therefore, the preloading force F_{pc} of each bolt is equal to:

$$F_{pc} = 0.7\, f_{ub} A_{res} = 134.4\, kN \tag{2}$$

According to Eurocode 3 [19,20], the sliding force $F_{s,Rd}$ is calculated through the following expression:

$$F_{s,rd} = \frac{k_s n_b n_s \mu}{\gamma_{M3}} F_{pc} \tag{3}$$

where:

- k_s is a coefficient that depends on the shape of the slotted hole (in the current case it is equal to 0.63);
- n_b is the number of bolts (5 in this case);
- n_s is the number of surfaces in contact (2 in this case);
- μ is the friction coefficient (herein assumed equal to 0.4);
- γ_{M3} is a safety factor equal to 1.25.

Equation (3) provided in the Code, is aimed at the design of connections in which the sliding is prevented until the ultimate limit state and therefore the coefficients k_s and γ_{M3} are used. Conversely, in the design of the connection herein presented, such coefficients are not taken into account.

Furthermore, concerning the preloading force, several studies in the literature show that the value of F_{pc} decreases progressively due to creep phenomena which is affected to high amount of preloading force applied to the bolt [21]. With the aim of limiting these effects, in [22,23] to contain the preloading force in the bolts within the range 30-60% of the maximum load suggested by the Code is proposed. Therefore, in the present study, the design sliding force $F_{s,d}$ is:

$$F_{s,d} = t_s n_b n_s \mu F_{pc} \tag{4}$$

where the parameter t_s is introduced for representing the stress level of the bolt, i.e. the aliquot of the maximum preload that is applied to the bolt and which is set between 0.3 and 0.6 as mentioned before. In particular, by equating Eq. (1) and Eq. (4) a stress level t_s=0.538 is obtained. Successively, the design preloading force $F_{pc,d}$ to be applied to each bolt is:

$$F_{pc,d} = t_s F_{pc} = 0.538 \cdot 134.4 = 72.3 kN \tag{5}$$

Based on these calculations and on the geometrical requirements provided in Eurocode 3 (CEN 2005a,b), the conception of the damping device is depicted in Fig. 2. Five bolts collocated on two rows are used

and curved slotted holes are designed, with rotation centre C indicated in the same figure. The main dimensions indicated are equal to: L_1 = 158 mm; L_2 = 342 mm; L_3 = 5 m; α=68° and β=22°.

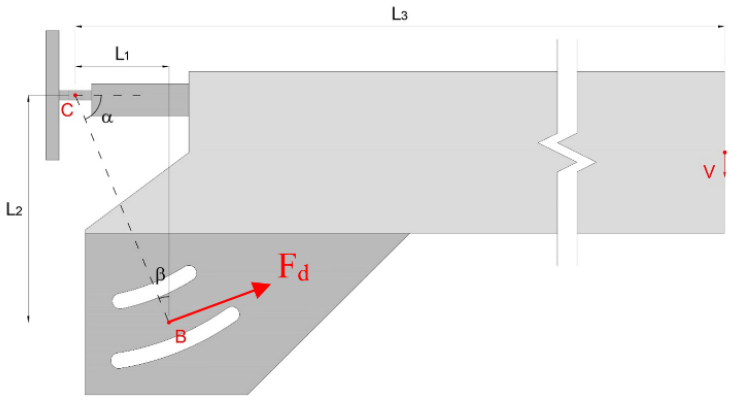

Fig. 2. Geometric scheme of the friction device.

It could be worth to observe that the design is conceived so that the diameter of the preloaded bolts can be easily changed providing the same preloading force given in Eq. (5) using a different stress level t_s. In this way it is possible to adopt HV bolt assemblies using the most common bolt diameters available in the market, for instance M16 or M20 bolts.

2.2 Dimensioning of the connections

The device is connected to the beam and the column through bolted steel plates, T-stub and angles which are depicted in Figs. 3 and 4. In particular, Fig. 3 shows the T-stub designed for the upper connection. The dimensions are the following: b_{fl} = 300 mm, h_{fl} = 200 mm, t_{fl} = 20 mm, t_w = 15 mm, b_w = 200 mm, l_w = 185 mm.

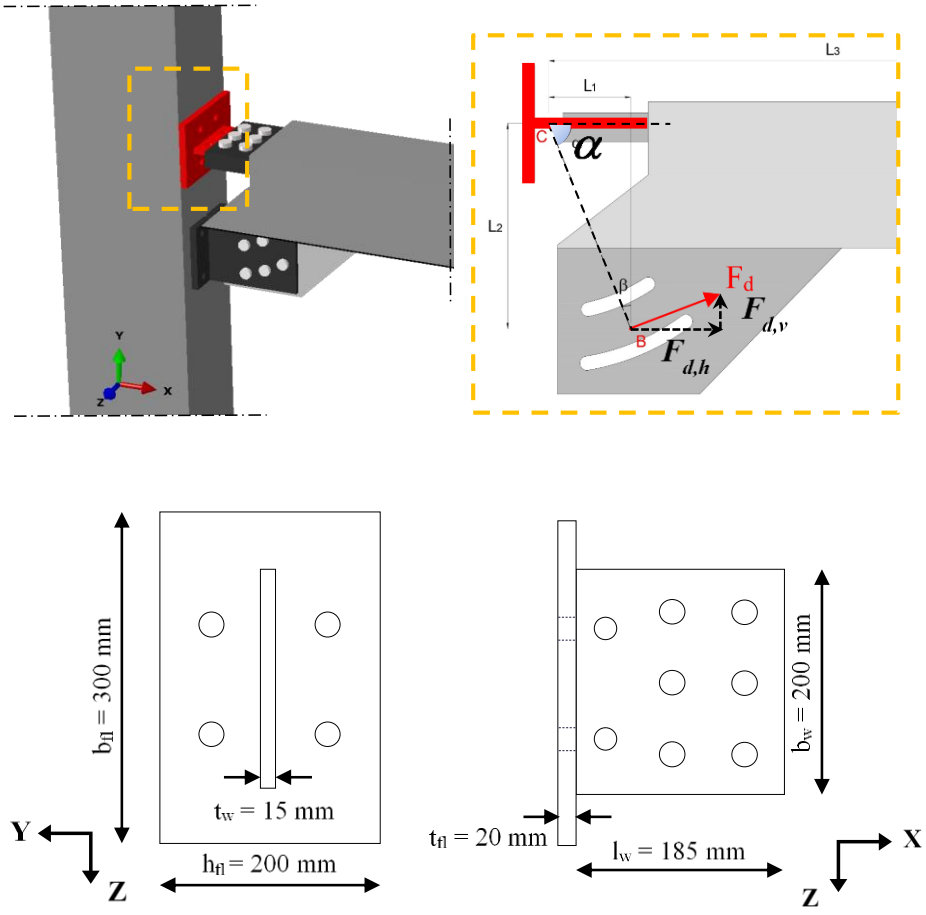

Fig. 3. Dimensions of the T-stub.

The connection between T-stub and beam is designed as a classical friction bolted connection where the design sliding force $F_{d,h}$ is evaluated as the horizontal component of the force defined in Eq. (1), i.e.:

$$F_{d,h} = \Omega_{\mu} F_d \sin(\alpha) = 402.6\ kN \tag{6}$$

α being the angle between the beam longitudinal axis and the axis connecting the rotation centre C and the application point of the sliding force B indicated in Fig. 2. For this connection, six M22 bolts of 10.9 class are used. The number of bolts required has been calculated through the following equation:

$$n_b = \frac{F_{d,h}\,\gamma_{M3}}{k_s n_s \mu F_{pc}} = \frac{402.6 \cdot 1.25}{1 \cdot 1 \cdot 0.4 \cdot 212.1} = 5.93 \Rightarrow 6 \tag{7}$$

The thickness of the T-stub web is dimensioned assuming that it must absorb only the traction expressed by Eq. (6) while the capacity to withstand the shear force is completely demanded to the steel angles of the lower connection depicted in Fig. 4.

The two lower steel angles are bolted to the slotted hole central plate. The dimensions of the angles are: h = 200 mm, b_{fl} = 80 mm, t_{fl} = 20 mm, t_w = 15 mm, l_w = 280 mm. The hole diameter is d_w = 19.5 mm; the holes are placed at a distance p_1 = 65 mm along each row while the distance between the two rows is p_2 = 90 mm.

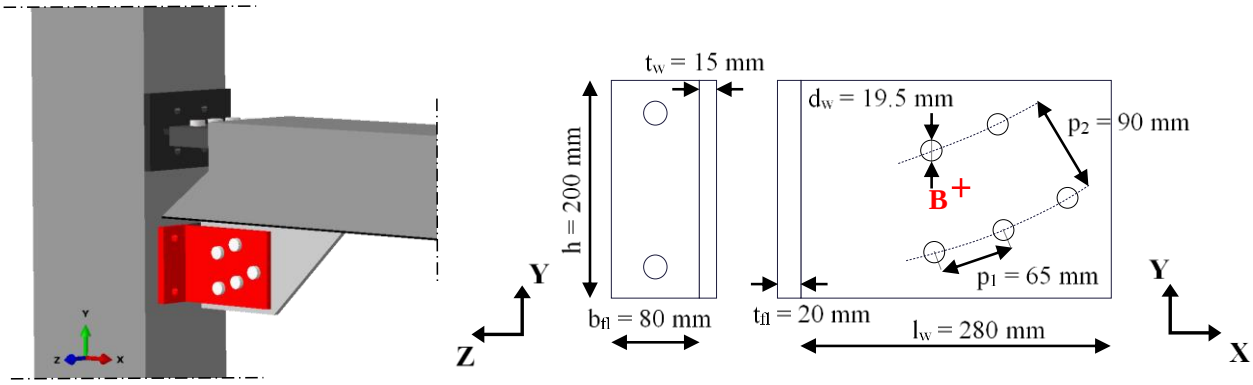

Fig. 4. Dimensions of the steel angle.

In the figure, the point B represents the centroid of the preloading forces of the five bolts.

Each angle is subjected to one half of the force expressed by Eq. (1) according to the horizontal and vertical components (B_0 and B_v respectively) which can be calculated through the following expressions:

$$B_o = \frac{1}{2}\Omega_\mu F_d \sin(\alpha) = 201.3\ kN \tag{8}$$

$$B_v = \frac{1}{2}\Omega_\mu F_d \cos(\alpha) = 81.4\ kN \tag{9}$$

Therefore, the web of the steel angle is dimensioned considering the bending moment in the presence of axial force while the flange is checked according to the plastic failure mechanisms of Eurocode 3 (CEN 2005a,b).

3 FINITE ELEMENT MODEL AND PRELIMINARY STUDIES

The feasibility study is conducted by means of the Finite Element Method (FEM) for the simulation of the structural behaviour of the dissipative connection. In this paper a first modelling approach is described, in which the structural details of the connection with column have not been investigated: the column is assumed to behave according to an unlimited elastic behaviour and the efficacy of the anchors is supposed to be perfect.

The FEM model consists of the assembly of different components, each of which has been experimentally tested in the past, while the effectiveness of FEM models in reproducing the results has been proven in various previously published papers. In particular, some of the authors already studied the most suitable modelling techniques for reproducing the flexural and shear behaviour of HSTCBs. In this regard, several researches have been published in the last few years such as [12] and [24] in which numerical models are developed and validated against experimental and analytical benchmarks. The model presented here is characterised by the main numerical and geometrical features of the studies mentioned above, but some characteristics were modified on the basis of preliminary FEM analyses that showed that the system exhibited no sufficient stiffness in the in-plane direction in the absence of inclined rebars welded on the lower plate of the HSTCB. Thus, the 12-mm diameter stirrups depicted in Fig. 5 were added. They have variable inclination and allow the activation of the stress transfer mechanism between concrete, steel top chord and slotted-hole central plate. Beam end shape and stirrup layout were chosen in order to reduce interferences with the slab after the concrete casting phase, and to ensure the replaceability of the T-stub and the bolts used in the connection with the C-shaped profile. For this reason, the area under the upper connection must be empty. At the same time, it is necessary to ensure a proper stress transfer capability between bottom and top chord of the steel truss connecting the two chords throughout the length of the connection. To fulfil the above requirement, the concrete core in the proximity of the connection presents an inclined external face throughout the length of the top bolted connection (see the beam profile shown in Fig. 1) and the layout of the inclined central stirrups is determined consequently. It is worth remarking that the number, inclination and position of the central

stirrups might be optimised through a parametric study aimed at reducing structural complexity and improving the stress transfer mechanism between the vertical central plate, the top and bottom chord of the steel truss, and the concrete core of the beam along the length of the device.

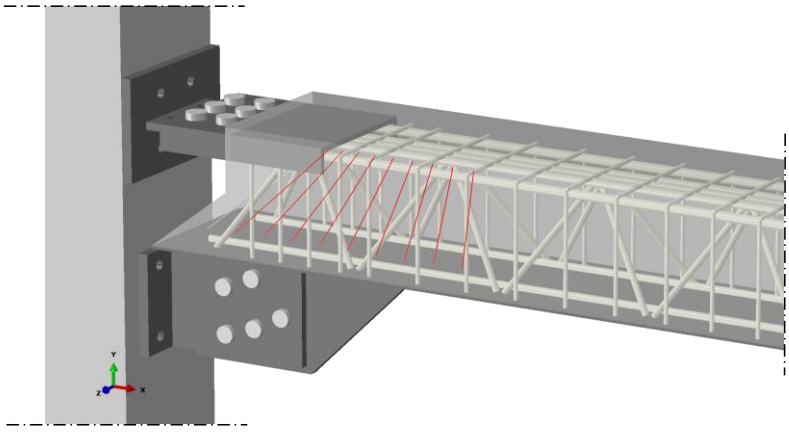

Fig. 5. Structural solution adopted for the simulation.

The preliminary FEM model took advantages of knowledge on several local phenomena (e.g. buckling of the web bars and steel plate, bonding between steel and concrete) affecting the behaviour of HSCTBs that have been thoroughly investigated over the last decade. More precisely, the phenomenon of buckling of the web bar of the steel truss of the HSTCB was analytically and experimentally investigated in several published researches such as [13,26]. Regarding buckling of the steel plate, a FEM analysis, not reported in the paper, on a beam model with larger stirrup spacing at the beam-end highlighted the possibility of triggering this phenomenon. Therefore, in order to prevent buckling in the bottom plate of the beam, the stirrup spacing was suitably reduced on the basis of simple analytical models proposed in Eurocode 3 for slender compressed members. Furthermore, it should be noted that the presence of the vertical web of the friction device and the additional bars welded to the plate ensure that the buckling phenomenon is prevented.

With regard to bonding between materials and pinching effect, numerous studies have already been carried out by some of the authors. In particular, modelling of bonding between steel reinforcement and concrete in HSTCBs was extensively studied in [13,15,16] and [27].

The main features of the final model are reported in Fig. 6. The response of the beam-to-column connection is reproduced assuming for the column a cross-section of 300x400 mm and a length of 3 m. The column has pinned supports and a cyclic displacement of ±100 mm is applied to the beam tip. More in detail, the length of the beam is 2.6 m, while the load application point is placed 2.4 m from the column face. Before application of the displacement history, the preloading force is applied to the bolts of the damping device. The finite elements used are represented in Fig. 7. In particular, first order tetrahedral are used for all components with the exception of column and C steel profile for which linear bricks are selected. The model is basically focused on the simulation of contacts. In particular, the friction formulation is adopted imposing the value of the friction coefficient between two adjacent surfaces in the damping device. Conversely, friction is assumed negligible between the bottom steel plate and the concrete of the HSTCB as well as between the concrete and the "C" profile partially embedded within the beam for ensuring the upper connection. Finally, perfect bond is assumed for the contact between concrete and diagonal, longitudinal and transversal reinforcement of the HSTCB (Fig. 8).

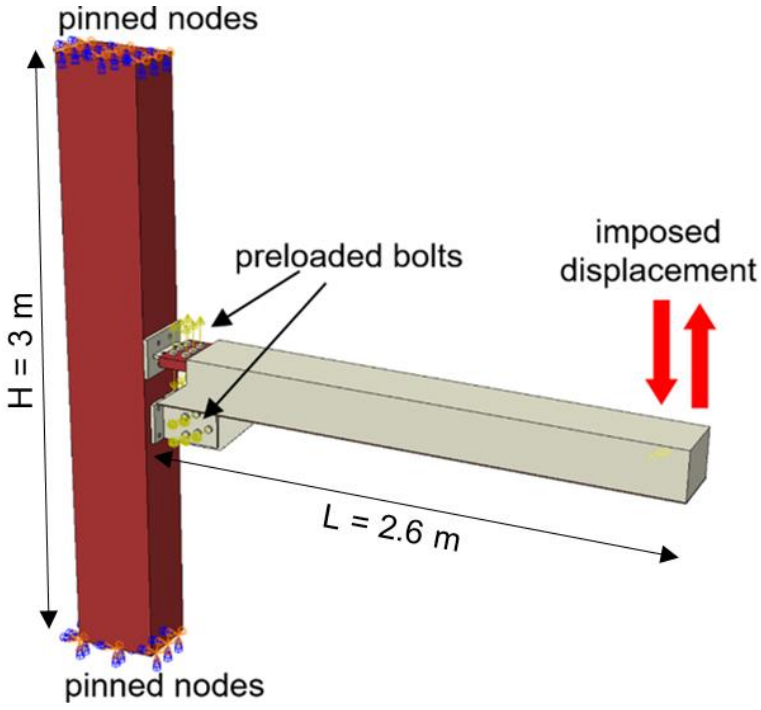

Fig. 6. Boundary and loading conditions.

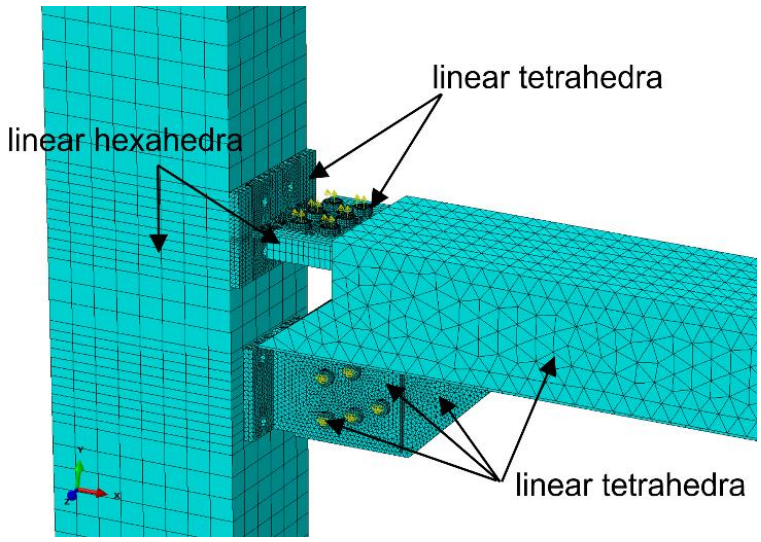

Fig. 7. Mesh of the elements.

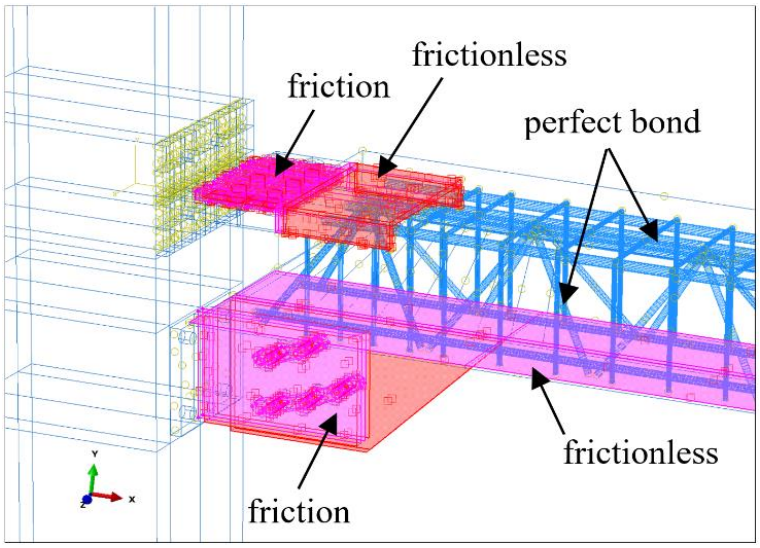

Fig. 8. Surfaces for the definition of contacts.

As regards materials, the steel elements are modelled using an elasto-plastic behaviour whose main features are reported in Table 1. In particular the table reports the elastic modulus (E_s), the yield stress (f_y) and the ultimate strain (ε_u) for each component of the friction device. For the concrete material, a compressive strength of 25 MPa and an elastic modulus of 28960 MPa have been adopted. The plastic behaviour of concrete is modelled using the Concrete Damaged Plasticity model based on the theory of plastic continuous damage of quasi-brittle materials. The overall stress-strain curve reported in Fig. 9 has been implemented.

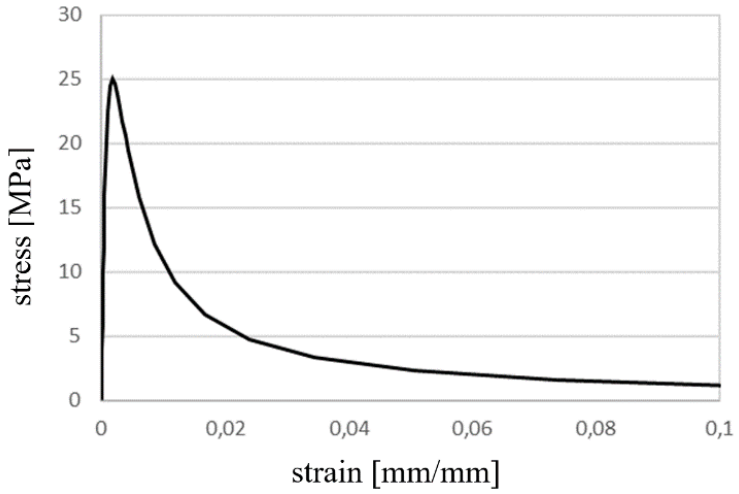

Fig. 9. Compressive stress-strain law of concrete.

	E_s [GPa]	f_y [MPa]	ε_u [%]
plates	210	355	0.3
bolts	210	900	0.3

Table 1. Mechanical features of the steel of the device.

An ulterior preliminary FEM analysis was performed aimed at reproducing the behaviour of the friction device already tested in the literature by [25] endowed with the friction pad "M2." The purpose of this analysis was validating the ability of the model in reproducing the mechanical response of a friction damper under traction, i.e. the friction sliding mechanism. In Fig. 10 the 3D FE model of the above-mentioned friction device is shown, while in Fig. 11 the comparison between experimental and numerical results is presented, proving the reliability of the employed modelling technique.

Regarding ulterior FEM model validation, it is well known that finite element models are often used as a preliminary tool for validating designing and calibration of structural elements designed on the basis of simple or sophisticated analytical models, as well as designing and calibrating the specimen of a structural element to be tested. Thus, the ability of FEM models to reproduce the behaviour of analytical calculations represent a further validation tool for the numerical model.

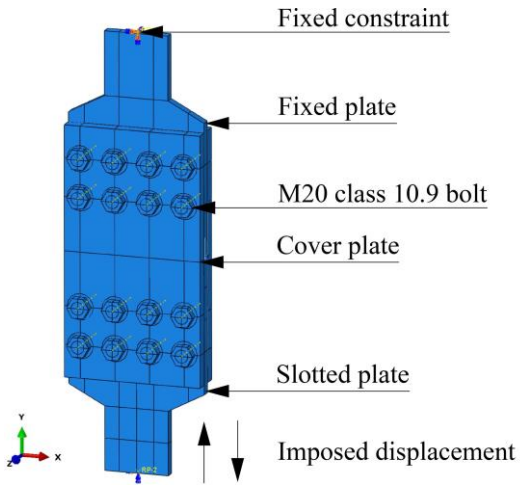

Fig. 10. 3D FE model of the friction device tested in Latour et al. (2015).

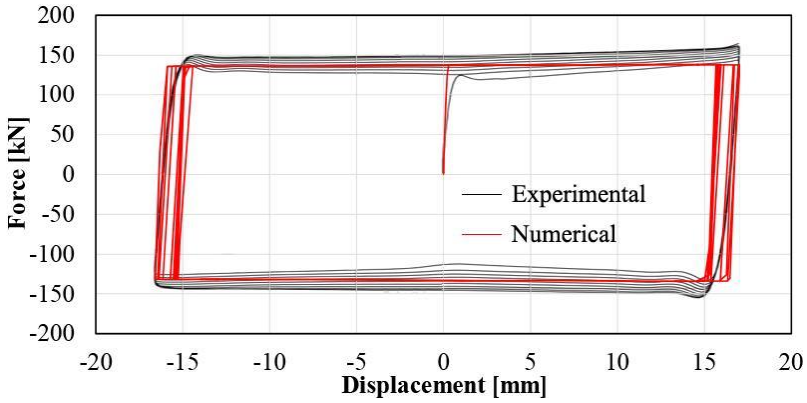

Fig. 11. Comparison between experimental and numerical results of the friction device endowed with the friction pad "M2" tested in Latour et al. (2015)

4 RESULTS

The results of the proposed connection are presented in terms of load-displacement curves and stress contours for both monotonic and cyclic response. Two analyses were performed, considering a design value of the bending moment equal to 1 and 1.5 times the value assumed in Section 2.1, respectively. The increment of the value of the bending moment was obtained by changing the preload acting on the bolts of the friction device. Fig. 12 reports the monotonic load-displacement plot. It can be observed that the system is able to provide the expected response. As a matter of fact, the resisting moment of the connection shown by the FEM model is in good agreement with the corresponding design value calculated analytically. In discussing the results in detail, three phases can be identified:

− Phase 1: the friction device does not slip; the behaviour of the system is almost elastic without relevant changes in stiffness;

− Phase 2: the sliding is activated and the behaviour of the system turns into plastic type, exhibiting a slight hardening probably due to the plasticization of the upper connection. The deformations of the beam slightly move the rotation centre assumed during the design;

− Phase 3: the design displacement limit is reached; a progressive increment in load is caused by the contact between the bolt shank and the slotted hole internal surfaces.

Fig. 13 reports the stress state in the device during the analyses between phase 1 and 2. The figure shows that all steel components of the device are in the elastic range of their constitutive behaviour. Moreover, the stress state seems to increase proportionally in all steel components when the moment strength is increased, proving the efficiency of the design procedure. In addition, it can be noticed that the inclined bars are effective in connecting the friction device to both the top chord and the concrete beam.

Similarly, the stress state in the concrete block is represented in Fig. 14. In particular, the minimum principal stresses are represented. The compression levels achieved are satisfactory in the whole concrete volume with the exception of the stress localization within the circled area in the Fig. 14b, where the bottom steel plate of the HSTCB is not effective in transferring the internal forces coming from the slotted hole plate.

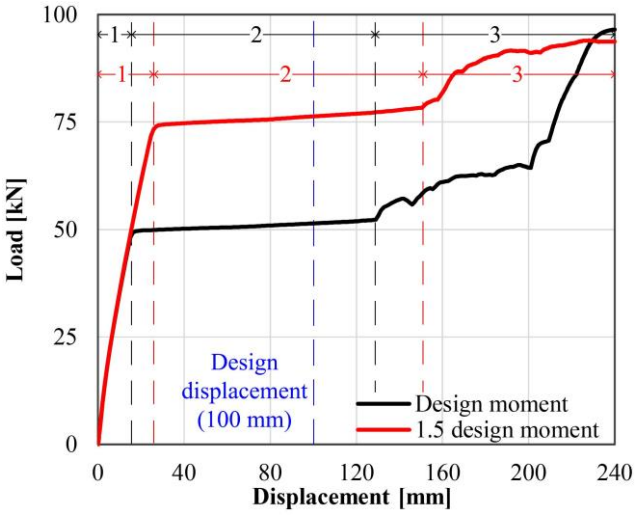

Fig. 12. Monotonic load-displacement curve.

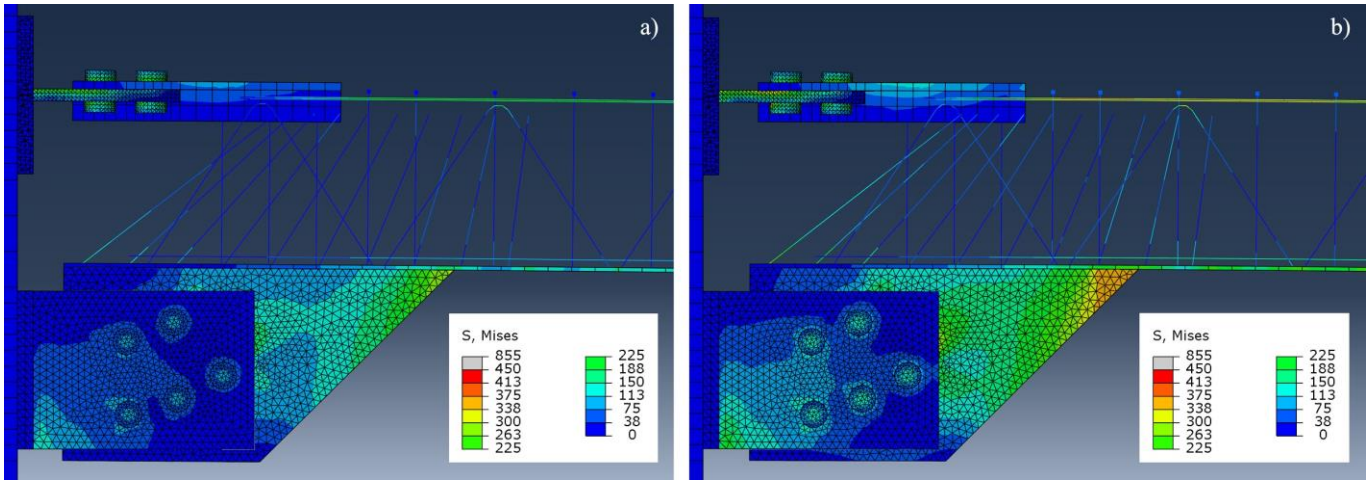

Fig. 13. Stress state in the steel elements between phase 1 and 2 of the analyses with M_d = 110 kNm (a) and 165 kNm (b).

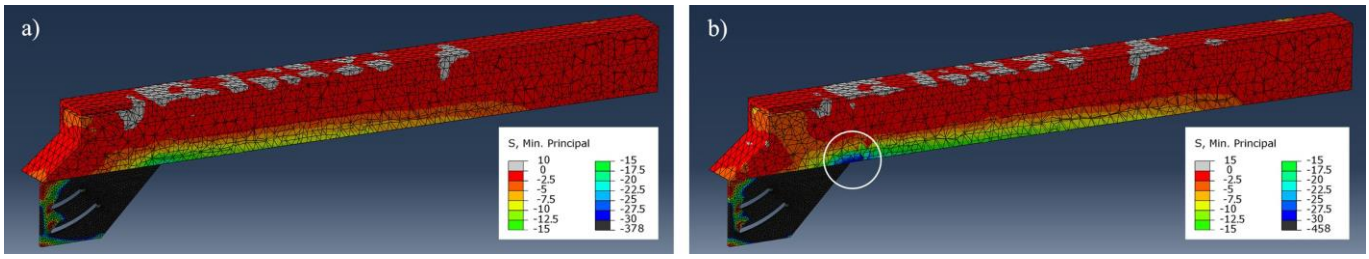

Fig. 14. Minimum principal stresses in the concrete between phase 1 and 2 of the analyses with M_d = 110 kNm (a) and 165 kNm (b).

In Fig. 15 the plastic maximum principal strains in the concrete are depicted. Three different cracked areas can be individuated for both the analyses:

− outer boundaries of the beam, i.e. beam extrados (1): here the concrete cracking is due to the flexural tensile stresses;

− concrete cover of the C steel profile (2): the deformations of the steel profile induce the damage of the concrete cover;

− bottom plate-concrete interface (3): the bottom steel plate and the concrete surfaces in contact experience damage because of the significant tensile stresses due to the inclined stirrups.

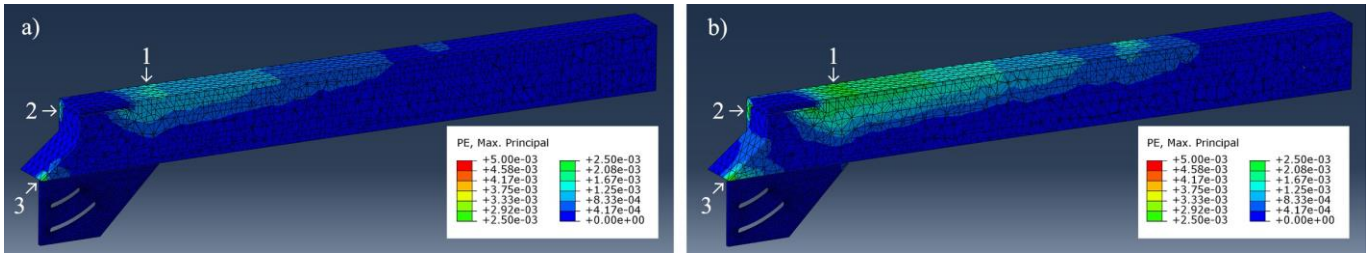

Fig. 15. Maximum principal strains in the concrete between phase 1 and 2 of the analyses with M_d = 110 kNm (a) and 165 kNm (b).

Similarly, it is possible to analyse the numerical output in the transition between phase 2 and 3 previously reported in Fig. 12. In particular, Fig. 16a and Fig. 16b show the stress state in the steel device for the analyses with M_d = 110 kNm and 165 kNm, which can be compared with Fig. 13a and Fig. 13b, respectively. The stress level in the steel elements is almost unchanged, except for the T-stub and the "C" profile: the increase of the rotation of the system produces the increase in the flexure to which the two elements are subjected. It can also be highlighted that the bending moment experienced by the "C" profile contributes to a slight shifting of the position of the centre of rotation from the assumed one. Nevertheless, the connection behaves according to the design requirements for displacement greater than the design one.

In the same way, the minimum principal stresses in the concrete of the two analyses shown in Figs. 17a and 17b are almost unchanged if compared to those of Figs. 14a and 14b, respectively, proving the capability of the friction connection to limit the forces to which the surrounding elements are subjected and preventing them from experiencing any plastic deformation.

Finally, Fig. 18 shows the cracked concrete in the transition between phase 2 and 3. In particular, the maximum principal strain contour indicates that there is a slight increment of the crack propagation especially in the area next to the C steel profile embedded within the concrete. This phenomenon might be due to the significant increment of the flexure of the "C" profile, despite its high stiffness. Such a flexure induces a progressive degradation of the concrete cover around the steel profile. Moreover, the cracking state at the beam extrados in the analysis with M_d = 110 kNm (Fig. 18a) seems to increase significantly if compared to that of Fig. 15a. By contrast, the cracking state at the beam extrados in the

analysis with M_d = 165 kNm (Fig. 18b) increases negligibly if compared to that in Fig. 15b. Therefore, the limitation in the concrete strain proves that there is no condition for which the pinching phenomenon could be activated.

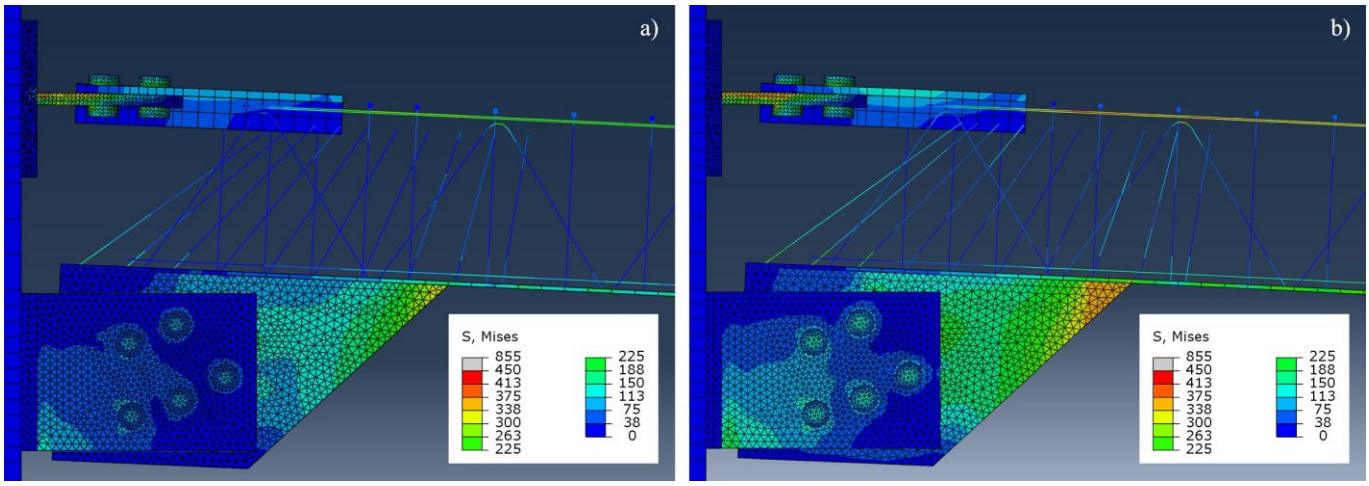

Fig. 16. Stress state in the device between phase 2 and 3 of the analyses with M_d = 110 kNm (a) and 165 kNm (b).

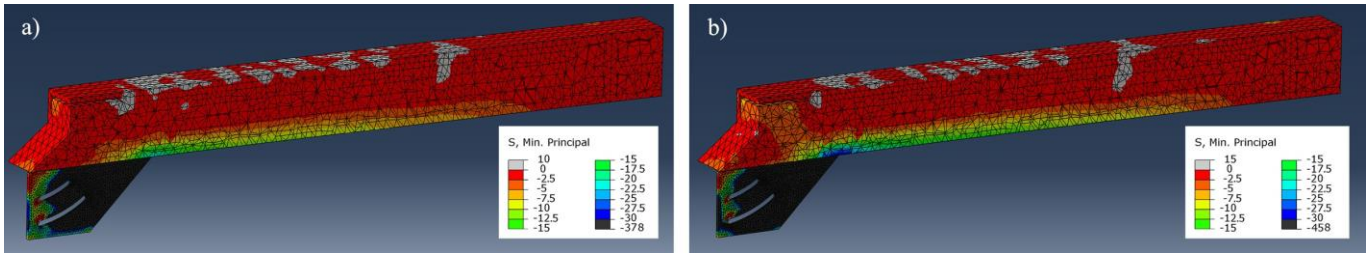

Fig. 17. Minimum principal stresses in the concrete between phase 2 and 3 of the analyses with M_d = 110 kNm (a) and 165 kNm (b).

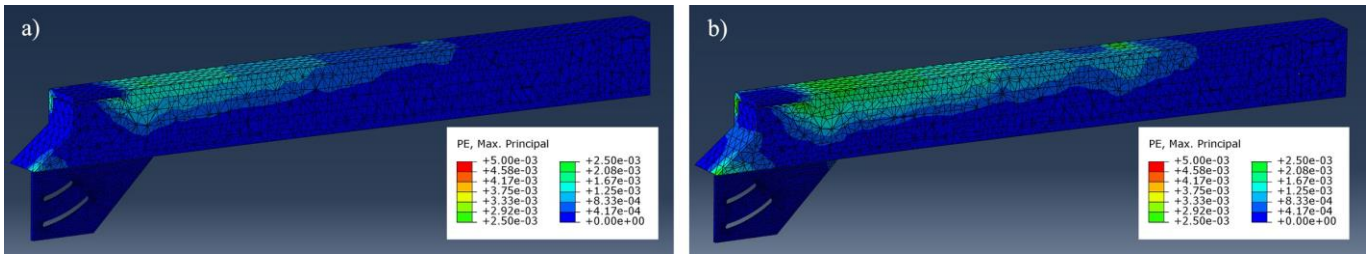

Fig. 18. Maximum principal strains in the concrete between phase 2 and 3 of the analyses with M_d = 110 kNm (a) and 165 kNm (b).

The output of Phase 3 is not analysed because it refers to the behaviour of the device beyond the design working condition.

The cyclic response is reported in Fig. 19. From the load-displacement curve reported in the figure, it can be observed that the system behaves according to the design requirements, i.e. it exhibits a symmetric response for hogging and sagging bending moments and does not evidence any damage in the loading-unloading phases. The analysis of the stress state is the same as already described for the monotonic numerical test. Although the FE analysis is not able to take into account the wearing of the friction pads and possible variation of the friction coefficient, the stability of the hysteresis cycles of the frictional dissipative connections, as attested by several papers in the literature (e.g. [2]), can be obtained through a combination of low-wear materials able to maintain the friction connection as constant as possible [28] and disk springs able to keep constant the value of the preload acting on the bolts of the connection [29]. Moreover, numerous experimental tests available in the literature prove the dissipative capacities and fatigue strength of the T-stub as described in [25].

With regard to the plasticization cumulated on the device components at the end of the cyclic test, Fig. 20 reports the distribution of the equivalent plastic strains in the steel elements of the analyses with moment strength equal to 110 kNm (a) and 165 kNm (b): it can be observed that all steel elements of the former are in the elastic range with the exception of the horizontal flange of the T-stub which behaves in the plastic range according to the design requirements. The latter also shows slight plasticization of the bottom plate and two of the inclined bars at the connection with the vertical central plate, due to the high stresses transferred, as already described in Figs. 14 and 17.

Concerning the concrete block, it can be noteworthy to assess the cracking state of the material on the basis of the equivalent tensile plastic strains represented in Fig. 21a and Fig. 21b for the analyses with M_d = 110 kNm and 165 kNm, respectively. As expected, in the inner rim of the beam, at its intrados, the concrete cracks when the beam is subjected to positive bending moment. In the same time, the cyclic action produces a greater deformation of the C steel profile of the upper connection with respect to the behaviour observed in the monotonic simulation, increasing the plastic strains of the surrounding concrete cover, leading to localized damage to the concrete corner in the first analysis, and to extensive damage concerning almost the whole concrete cover of the "C" profile in the second one. This phenomenon is due to the combination of the thin concrete cover and the deformability of the "C" profile.

In addition, slight damage to the concrete cover is also registered in Fig. 21b at the connection between the bottom plate and the part of the concrete beam with the inclined shape, due to the forces transferred by the inclined bars. However, all the above-mentioned concrete damages are minor and do not influence the cyclic performance of the proposed connection.

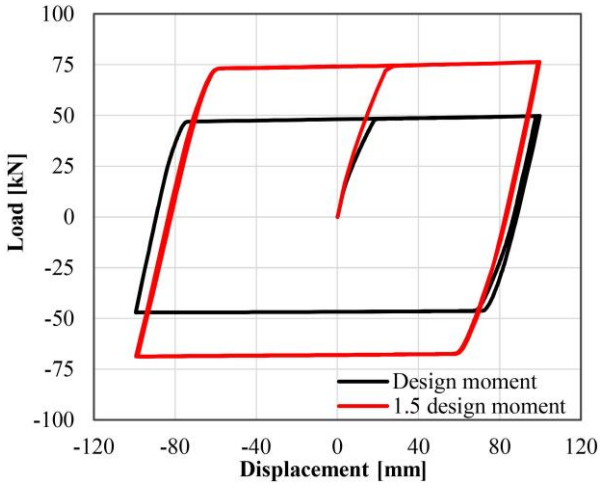

Fig. 19. Cyclic load-displacement curve.

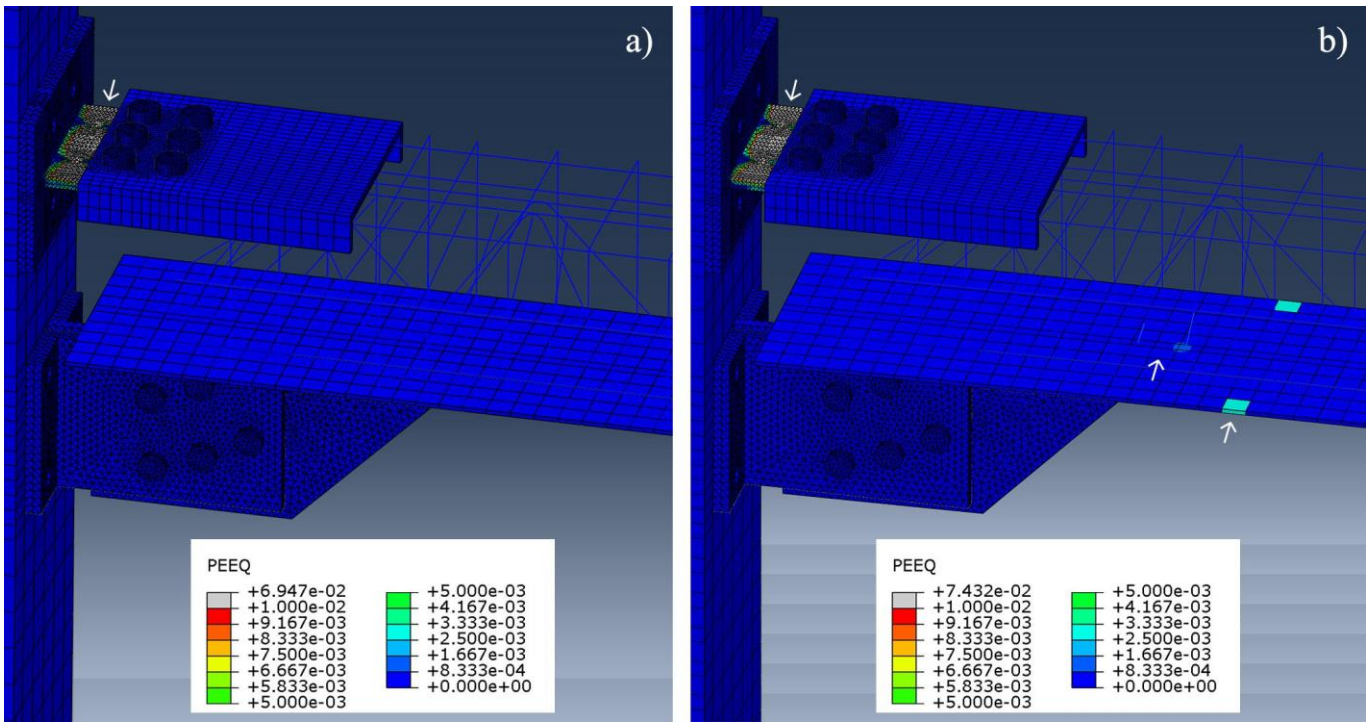

Fig. 20. Plastic strain distributions at the end of the cyclic FE tests with M_d = 110 kNm (a) and 165 kNm (b).

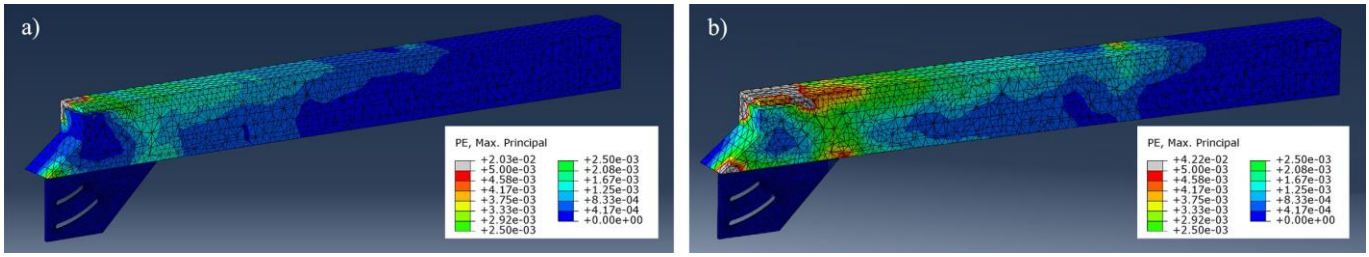

Fig. 21. Maximum principal strains in the concrete at the end of the cyclic FE tests with M_d = 110 kNm (a) and 165 kNm (b).

Table 2 summarises the numerical results obtained in terms of peak stress and strain values referred to specific parts of interest of the model. In particular, for each component of the structural system, the stress and strain values are referred to the following areas:

- concrete: the contact area with the right end of the slotted-hole plate and the upper part near the connection with the C profile;
- slotted-hole plate: the right end of the plate in contact with the bottom plate of the beam;
- steel angle: the base section;
- T-stub: the area between the base section and the first row of bolts starting from the column;
- C profile: the area between the second row of bolts starting from the column and the mid-section of the profile.

It should be noted that the peak stress and strain values do not consider the areas subjected to the bolt preload.

	M_d =110 kNm				**M_d = 165 kNm**			
	transition step phase 1 - 2		*transition step phase 2 - 3*		*transition step phase 1 - 2*		*transition step phase 2 - 3*	
	$\sigma_{max/min}$ [MPa]	$\varepsilon_{max/min}$ [%]	$\sigma_{max/min}$ [MPa]	$\varepsilon_{max/min}$ [%]	$\sigma_{max/min}$ [MPa]	$\varepsilon_{max/min}$ [%]	$\sigma_{max/min}$ [MPa]	$\varepsilon_{max/min}$ [%]
concrete	2.46	0.14	2.34	0.15	2.45	0.24	2.29	0.26
	-21.5	-0.08	-22.3	-0.08	-28.7	-0.12	-29.5	-0.13
slotted-hole plate	-	0.05	-	0.05	-	0.13	-	0.15
	-340	-0.15	-365	-0.16	-445	-0.3	-463	-0.33
steel angle	17.2	0.03	7.25	0.02	26.2	0.04	16.7	0.04
	-157	-0.07	-145	-0.07	-236	-0.11	-223	-0.1
T-stub	365	0.16	520	0.64	423	0.25	550	0.9
	-62.3	-0.03	-380	-0.29	-91.7	-0.1	-415	-0.55
C profile	178	0.07	183	0.08	275	0.12	282	0.13
	-19.4	-0.01	-54.5	-0.03	-28.3	-0.01	-64.1	-0.04

Table 2. Peak stress and strain values of the monotonic response with M_d =110 kNm and M_d = 165 kNm

From the Table, it can be observed that the maximum stress in the concrete material is less than the peak value (2.56 MPa) because the cracking of the top concrete was already achieved in previous steps of the analysis. Conversely, the minimum stress for M_d=165 kNm goes over the peak compressive stress implemented for describing the monotonic behaviour because of the biaxial compressive state present in the analysed area of concrete. As regards the steel members, the minimum stresses in the slotted hole plate slightly increase between the two considered numerical steps in both analyses, proving that, during the sliding of the system, the stress state of the components of the friction device are substantially unchanged. The minimum stress and strain values in the steel angles and the maximum values in the C-profile in the considered transition steps of the two analyses, are almost directly proportional. Finally, the maximum stresses and strains in the T-stub show the formation of the plastic hinge after the transition step from phase 1 to phase 2 and subsequently the hinge is able to work as rotation centre of the system as supposed during the design process.

Figs. 22a, 22b show the distribution of shear in the nodal area due to the hogging and sagging moments once the sliding force of the friction device is achieved. Such shear distribution is qualitatively comparable with the literature results reported in [5], proving the reliability of the presented model.

In particular, Fig. 22 shows that the shear forces to which the elements in the nodal area are subjected achieve values well beyond the shear acting on the beam, the latter corresponding to the force applied on the beam tip, and follow complex distribution, requiring particular attention during the design procedure. With regard to the hogging moment analysis (Fig. 22a), it can be noticed that the shear experienced by the vertical central plate is more than twice the shear acting on the beam. To preserve the vertical equilibrium, the beam segment at the connection with the friction device is subjected to shear force, with opposite sign, almost twice that acting on the remaining length of the beam. Regarding the connection elements to the column, it can be seen that the shear acting on the steel angles is higher than that acting on the beam and, thus, in order to preserve the vertical equilibrium, the T-stub is subjected to shear force with opposite sign. Concerning the sagging moment analysis (Fig. 22b), the shear distribution is similar to the previous one, but with the opposite sign. With regard to the shear force absorbed by the inclined

bars, it can be seen that only the bars placed at the beginning and at the end of the vertical central plate are subjected to shear force, while the group of bars in the middle experience negligible shear force, as confirmed by the stress state of the steel elements reported in Figs. 13 and 16.

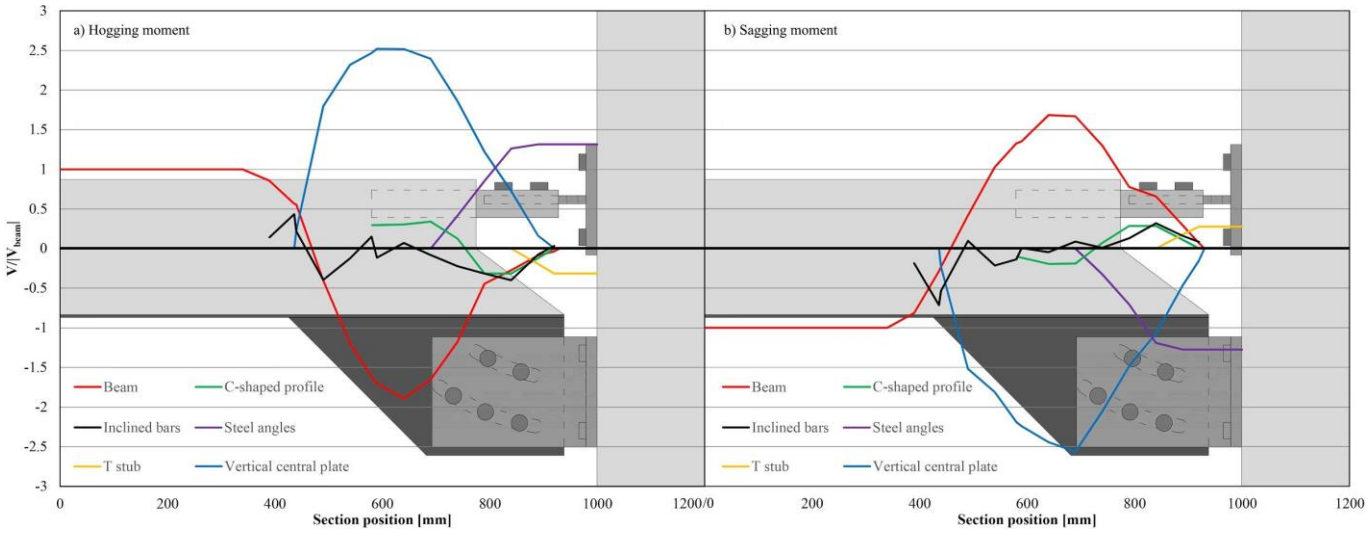

Fig. 22. Distribution of shear in the nodal area due to the hogging and sagging moments once the sliding force of the friction device is achieved.

5 CONCLUSIONS

In this study the introduction of friction dampers in the HSTCB-to-column joints of framed structures has been investigated. The calculation has been conducted according to the current prescriptions for buildings in seismic areas and the damping device has been adequately designed for its application on R.C. frames. The friction device components and the connections to beam and column have been dimensioned and verified according to Eurocode 3 prescriptions. Conversely, the structural details of the column and the connection within the latter have been neglected, in the meaning that the column behaviour has been assumed linear elastic and the efficacy of the anchors perfect.

The device has been conceived for a working level of the preloaded bolts of 0.54 adopting an overstrength coefficient of 1.5.

The feasibility study has been firstly conducted through the development of design criteria for the pre-dimensioning of the device and, successively, the proposed solution has been validated through the

generation of finite element models. With regard to the design of the geometry of the friction connection, an iterative procedure was employed aiming at minimizing the height of the vertical central plate.

The FEM model consisted of the assembly of different components, each of which was experimentally tested, and the effectiveness of FEM models in reproducing the results was proven in various previously published papers.

Monotonic and cyclic tests were simulated; for each of these, two analyses were carried out, considering a design value of the bending moment equal to 1 and 1.5 times the value assumed for design of the friction connection, i.e. 110 kNm. The increment of the value of the bending moment is obtained by changing the preload acting on the bolts of the friction device. To assess the performances of the proposed connection, global and local results, such as force-displacement response of the subassembly and stress and strain state in steel element and concrete beam, were investigated. The results of the monotonic analyses provide force-displacement curves characterized by plastic behaviour with slight hardening, once the sliding force is achieved, up to displacement values well beyond the design one. With regard to the stress state of the steel elements, the results show that all the components constituting the connection behaved according to the design requirements. In particular, the steel elements remain elastic with the exception of the T-stub components in which the rotation centre of the system was theoretically assumed during the design process. Concerning the stress state of the concrete beam, a stress concentration at the connection between vertical central plate and concrete beam was registered, but with stress values that did not exceed the compressive strength of concrete even in the analysis with M_d = 165 kNm. Moreover, three different areas subjected to cracking are highlighted, i.e. the beam extrados, the concrete cover of the "C" profile and the bottom plate-concrete beam interface. The cracking amplitude values were small, proving the capability of the friction connection to limit the forces, and thus the plastic deformations, experienced by the surrounding elements.

The cyclic behaviour showed a symmetric response under hogging and sagging bending moment without degradation during the unloading and reloading phases. As a matter of fact, all the steel elements behaved in the elastic range except the horizontal flange of the T-stub and, only in the analysis with M_d = 165 kNm, the inclined bars and the bottom plate at the connection between the vertical central plate and the

concrete beam. Concerning the cracking state at the end of the cyclic analyses, only minor damage was registered at the concrete cover of the "C" profile and, only in the analysis with M_d = 165 kNm, at the connection between the bottom plate and the part of the concrete beam with the inclined shape.

Lastly, the analysis of the shear distribution in the nodal area for hogging and sagging moments once the sliding force of the friction device is achieved highlighted that the shear forces to which the elements in the nodal area are subjected achieve values well beyond the shear acting on the beam. More precisely, the shear forces acting on the vertical central plate, the beam segment at the connection with the friction device and the steel angles are almost equal to 2.5, 2 and 1.3 times the shear force acting on the remaining length of the beam, respectively. This outcome requires that particular attention be given to the shear strength of elements during the design procedure.

Future improvements of the solution could concern simplification of the connection of the vertical central plate to the concrete beam and the steel top chord, optimization of the number and position of the inclined bars, detailing of the device-to-column connection, assembly procedure and tolerances, and slab interactions. In this regard, in order to accommodate the interaction between the slab and the connection, a group of slotted holes arranged in the radial direction could be inserted in the plates of steel angles connected to the vertical central plate. Lastly, details of the construction process, the assembly procedure and the related dimensional tolerances have to be investigated in more detail with the aim of using the proposed connection in the construction industry.

ACKNOWLEDGEMENTS

The economic support to the research of the SICILFERRO TORRENOVESE s.r.l. company is acknowledged, and the Authors thank Dr. Mauro Scurria and Eng. Nicolò Cancelliere for helpful discussion and active participation in the research project.

REFERENCES

[1] Chanchi Golondrino JC, MacRae GA, Chase JG, Rodgers GW, Clifton GC. Asymmetric Friction Connection (AFC) Design for Seismic Energy Dissipation. J Constr Steel Res 2019;157:70-81. https://doi.org/10.1016/j.jcsr.2019.02.027.

[2] Khoo HH, Clifton C, Macrae G, Zhou H, Ramhormozian S. Proposed Design Models for the Asymmetric Friction Connection. Earthq Eng Struct Dyn 2015;44(8):1309-24. https://doi.org/10.1002/eqe.2520.

[3] Ramhormozian S, Clifton GC, MacRae GA, Khoo HH. The sliding hinge joint: final steps towards an optimum low damage seismic-resistant steel system. Key Eng Mater 2018;763:751-60. https://doi.org/10.4028/www.scientific.net/KEM.763.751.

[4] Latour M, Piluso V, Rizzano G. Experimental analysis of beam-to-column joints equipped with sprayed aluminium friction dampers. J Constr Steel Res 2018;146:33-48. https://doi.org/10.1016/j.jcsr.2018.03.014.

[5] Latour M, D'Aniello M, Zimbru M, Rizzano G, Piluso V, Landolfo R. Removable friction dampers for low-damage steel beam-to-column joint. Soil Dyn Earthq Eng 2018;115:66-81. https://doi.org/10.1016/j.soildyn.2018.08.002.

[6] Morgen BG, Kurama YC. A friction damper for post-tensioned precast concrete moment frames. PCI J 2004;49(4):112-33. https://doi.org/10.15554/pcij.07012004.112.133.

[7] Tsampras G, Sause R, Fleischman RB, Restrepo JI. Experimental study of deformable connection consisting of friction device and rubber bearings to connect floor system to lateral force resisting system. Earthq Eng Struct Dyn 2018;47(4):1032-53. https://doi.org/10.1002/eqe.3004.

[8] Zhang Z, Fleischman RB, Restrepo JI, Guerrini G, Nema A, Zhang D, Shakya U, Tsampras G, Sause R. Shake-table test performance of an inertial force-limiting floor anchorage system. Earthq Eng Struct Dyn 2018;47(10):1987-2011. https://doi.org/10.1002/eqe.3047.

[9] Colajanni P, La Mendola L, Monaco A. Stiffness and Strength of Composite Truss Beam to R.C. Column Connection in MRFs. J Constr Steel Res 2015;113:86-100. https://doi.org/10.1016/j.jcsr.2015.06.003.

[10] Colajanni P, La Mendola L, Monaco A, Spinella N. Cyclic Behavior of Composite Truss Beam-to-RC Column Joints in MRFS. Key Eng Mater 2016;711:681-9. https://doi.org/10.4028/www.scientific.net/KEM.711.681.

[11] Colajanni P, La Mendola L, Monaco A. Experimental Investigation on the Shear Response of Precast Steel-Concrete Trussed Beams. J Struct Eng ASCE 2017;143(1):04016156. https://doi.org/10.1061/(ASCE)ST.1943-541X.0001642.

[12] Monaco A. Numerical Prediction of the Shear Response of Semi-Prefabricated Steel-Concrete Trussed Beams. Constr Build Mater 2016;124:462-74. https://doi.org/10.1016/j.conbuildmat.2016.07.126.

[13] Colajanni P, La Mendola L, Latour M, Monaco A, Rizzano G. FEM Analysis of Push-out Test Response of Hybrid Steel Trussed Concrete Beams (HSTCBs). J Constr Steel Res 2015;111:88-102. https://doi.org/10.1016/j.jcsr.2015.04.011.

[14] Colajanni P, La Mendola L, Latour M, Monaco A, Rizzano G. Analytical Prediction of the Shear Connection Capacity in Composite Steel–concrete Trussed Beams. Mater Struct 2017;50(1):48. https://doi.org/10.1617/s11527-016-0931-4.

[15] Colajanni P, La Mendola L, Monaco A. Review of Push-out and Shear Response of Hybrid Steel-Trussed Concrete Beams. Buildings 2018;8(10):134. https://doi.org/10.3390/buildings8100134.

[16] Colajanni P, La Mendola L, Monaco A. Stress Transfer and Failure Mechanisms in Steel-Concrete Trussed Beams: Experimental Investigation on Slab-Thick and Full-Thick Beams. Constr Build Mater 2018;161(1):267-81. https://doi.org/10.1016/j.conbuildmat.2017.11.134.

[17] Priestley MJN, Sritharan S, Conley JR, Pampanin S. Preliminary Results and Conclusions From the PRESSS Five Storey Precast Concrete Test Building. PCI J 1999;44(6):42-67.

[18] Pampanin S, Amaris A, Akguzel U Palermo A. Experimental Investigations on High-Performance Jointed Ductile Connections for Precast Frames. Proceedings of the First European Conference on Earthquake Engineering and Seismology 2006. Geneva, Switzerland.

[19] CEN EN 1993-1-1-Eurocode 3: Design of Steel Structures. Part 1: General Rules and Rules for Buildings. Comité Européen de Normalisation, 2005.

[20] CEN EN 1993-1-8-Eurocode 3: Design of steel structures – Part 1-8: Design of joints, 2005.

[21] D'Antimo M, Latour M, Ferrante Cavallaro G, Jaspart JP, Ramhormozian S, Demonceau JF. Short- and long- term loss of preloading in slotted bolted connections. J Constr Steel Res 2020;167:105956. https://doi.org/10.1016/j.jcsr.2020.105956.

[22] Ferrante Cavallaro G, Francavilla A, Latour M, Piluso V, Rizzano G. Experimental behaviour of innovative thermal spray coating materials for FREEDAM joints. Compos Part B Eng 2017;115:289-99. https://doi.org/10.1016/j.compositesb.2016.09.075.

[23] Ferrante Cavallaro G, Latour M, Francavilla A, Piluso V, Rizzano G. Standardised friction damper bolt assemblies time-related relaxation and installed tension variability. J Constr Steel Res 2018;141:145-55. https://doi.org/10.1016/j.jcsr.2017.10.029.

[24] Ballarini R, La Mendola L, Le J, Monaco A. Computational study of failure of hybrid steel trussed concrete beams. J Struct Eng ASCE 2017;143(8):04017060. https://doi.org/10.1061/(ASCE)ST.1943-541X.0001792.

[25] Latour M, Piluso V, Rizzano G. Free from damage beam-to-column joints testing and design of DST connections with friction pads. Eng Struct 2015;85:219-33. https://doi.org/10.1016/j.engstruct.2014.12.019.

[26] Colajanni P, La Mendola L, Monaco A. Stress transfer mechanisms investigation in hybrid steel trussed-concrete beams by push-out tests. J Constr Steel Res 2014;95:56-70. https://doi.org/10.1016/j.jcsr.2013.11.025.

[27] Ballarini R, La Mendola L, Le J, Monaco A. 2020. Computational assessment of the structural performance of concrete beams with encased steel joist. Proceedings of the 6th European Conference on Computational Mechanics: Solids, Structures and Coupled Problems (ECCM 6), Glasgow (UK), 11-15 June 2018, Edited by: Roger Owen, René de Borst, Jason Reese and Chris Pearce, pp. 1187-1198, ISBN: 978-84-947311-6-7.

[28] Khoo HH, Clifton C, Butterworth J, MacRae G, Ferguson G. Influence of steel shim hardness on the Sliding Hinge Joint performance. J Constr Steel Res 2012;72:119-29. https://doi.org/10.1016/j.jcsr.2011.11.009

[29] Ramhormozian S, Clifton CG, MacRae GA, Davet GP, Khoo HH. Experimental studies on Belleville springs use in the sliding hinge joint connection. J Constr Steel Res 2019;159:81-94. https://doi.org/10.1016/j.jcsr.2019.03.031.

FIGURE CAPTIONS

Fig. 20 - Plastic strain distributions at the end of the cyclic FE tests with M_d = 110 kNm (a) and 165 kNm (b).

Fig. 21 - Maximum principal strains in the concrete at the end of the cyclic FE tests with M_d = 110 kNm (a) and 165 kNm (b).

Fig. 22 - Distribution of shear in the nodal area for hogging and sagging moment once the sliding force of the friction device is achieved.